

Crystal structure of a membrane-bound metalloenzyme that catalyses the biological oxidation of methane

Raquel L. Lieberman & Amy C. Rosenzweig

Departments of Biochemistry, Molecular Biology, and Cell Biology and of Chemistry, Northwestern University, Evanston, Illinois 60208, USA

Particulate methane monooxygenase (pMMO) is an integral membrane metalloenzyme that catalyses the conversion of methane to methanol. Knowledge of how pMMO performs this extremely challenging chemistry may have an impact on the use of methane as an alternative energy source by facilitating the development of new synthetic catalysts. We have determined the structure of pMMO from the methanotroph *Methylococcus capsulatus* (Bath) to a resolution of 2.8 Å. The enzyme is a trimer with an $\alpha_3\beta_3\gamma_3$ polypeptide arrangement. Two metal centres, modelled as mononuclear copper and dinuclear copper, are located in soluble regions of each pmoB subunit, which resembles cytochrome *c* oxidase subunit II. A third metal centre, occupied by zinc in the crystal, is located within the membrane. The structure provides new insight into the molecular details of biological methane oxidation.

The direct conversion of natural gas, composed primarily of methane, to useful fuels and chemicals represents a major challenge for chemistry and engineering. Efficient transformation of methane to a liquid such as methanol would make the extensive and under-used natural gas reserves a realistic alternative to petroleum, affecting worldwide energy use, the environment, and the economy¹. This chemical reaction is difficult to perform because methane is the most inert hydrocarbon (104 kcal mol⁻¹ C–H bond) and the desired product, methanol, reacts further at high temperature². Catalysts that overcome these obstacles have not yet been developed. By contrast, in nature, methane monooxygenase (MMO) enzymes convert methane to methanol at ambient temperature.

MMO is the first enzyme in the metabolic pathway of methanotrophs, which are bacteria that use methane as their sole source of carbon and energy³. Methanotrophs have been used to combat emissions of methane⁴, a potent greenhouse gas, and are also useful for bioremediation because they can oxidise halogenated hydrocarbons^{3,5}. Membrane-bound particulate MMO (pMMO), soluble MMO (sMMO)⁶, and the related enzyme ammonia monooxygenase (AMO)⁷ are the only known enzymes capable of methane hydroxylation. All methanotrophs produce pMMO, which is housed in intracytoplasmic membranes. Under copper-limiting conditions, several strains also produce sMMO³. The well-studied sMMO system comprises a hydroxylase (MMOH), a reductase and a regulatory protein⁶. The crystal structure of MMOH, which contains a carboxylate-bridged di-iron centre, has been known for a decade⁸. By contrast, most questions surrounding the biochemistry, structure and mechanism of the predominant methane oxidation enzyme, pMMO, have remained unanswered despite considerable research efforts in the last 20 years (ref. 9).

pMMO is composed of three subunits, pmoB (α , ~47 kDa), pmoA (β , ~24 kDa)¹⁰, and pmoC (γ , ~22 kDa)¹¹, each containing predicted membrane-spanning helices. The molecular mass and oligomerization state of pMMO are not established, but ~100-kDa $\alpha\beta\gamma$ (ref. 12) and 200-kDa $\alpha_2\beta_2\gamma_2$ (ref. 13) polypeptide arrangements have been proposed. The metal content of pMMO is controversial, with reported values of 2–15 copper ions^{12–16} and 0–2 iron ions^{13–16} per ~100-kDa purified pMMO.

Characterization of pMMO has led to three different models of the metal centre(s). Five trinuclear copper centres have been

proposed by Chan *et al.* on the basis of the hyperfine splitting pattern of an electron paramagnetic resonance (EPR) signal at $g = 2.06$, and have been hypothesized to fall into catalytic (C) and electron transfer (E) functional classes¹⁷. Other researchers, including ourselves, observe a type 2 mononuclear Cu(II) EPR signal only^{13,14,16,18}. DiSpirito and co-workers have suggested two copper and two iron ions with 6–8 additional copper ions bound to methanobactin, a siderophore-like molecule¹⁹, based on pMMO metal content and the isolation of methanobactin¹⁴. In addition to a mononuclear copper site, we have proposed a copper-containing cluster on the basis of extended X-ray absorption fine structure (EXAFS) data best-fitted with a 2.57-Å Cu–Cu interaction^{9,13}. To address these conflicting models and to provide a foundation for directed functional studies, we crystallized *Methylococcus capsulatus* (Bath) pMMO and report here the 2.8-Å resolution structure.

Overall architecture

The pMMO structure was solved by copper single-wavelength anomalous dispersion (SAD) (Supplementary Table S1 and Methods) and refined to 2.8-Å resolution. Three copies each of the pmoA, pmoB and pmoC subunits form a cylindrical $\alpha_3\beta_3\gamma_3$ trimer ~105 Å long and ~90 Å in diameter (Fig. 1a, b). A soluble region composed mainly of six β -barrel structures, two from each protomer, extends ~45 Å away from the membrane, and is supported by 42 transmembrane (TM) helices, 14 from each protomer. A hole is formed in the centre of the trimer (Fig. 1b). In the soluble region, this opening is ~11 Å in diameter and is lined with glutamic acid, aspartic acid and arginine residues. Although these residues stabilize the trimer, they are not conserved among pMMO homologues. The opening then extends into the membrane where it is lined with hydrophobic residues and widens to ~22 Å at the end opposite the soluble region.

The trimeric structure of pMMO was not anticipated and provides the first experimental evidence for a 1:1:1 subunit ratio. The molecular mass of multisubunit membrane proteins is difficult to determine accurately owing to the presence of detergents²⁰. Using nondenaturing gel electrophoresis techniques, we previously suggested a molecular mass of ~200 kDa for purified pMMO, probably corresponding to an $\alpha_2\beta_2\gamma_2$ polypeptide arrangement.

We also observed an ~400-kDa species under some conditions¹³. Chan and co-workers obtained a mass of ~220 kDa by analytical gel filtration, which they attributed to an ~100-kDa $\alpha\beta\gamma$ monomer in complex with 240 detergent molecules¹². Early electron micrographs of reconstituted membranes and two-dimensional crystals of pMMO from *M. capsulatus* (strain M) show a hexagonal particle ~9 nm in diameter with six maxima of protein density²¹. These maxima probably correspond to the six β -barrel structures in the soluble region of *M. capsulatus* (Bath) pMMO (Fig. 1b), suggesting that the crystallographically observed trimer is physiologically relevant.

Protomer structure

Each protomer in the trimer comprises single copies of the pmoB, pmoA and pmoC subunits (Fig. 2a). Consistent with N-terminal sequencing results^{10,13}, pmoB includes residues 33–414. The first 32 residues are proposed to be a leader sequence¹⁰. The soluble regions are derived primarily from pmoB and include two antiparallel β -barrel structures, one at the N terminus and the other at the C terminus (Fig. 2b). The N-terminal β -barrel is composed of seven strands, and is oriented ~90° from the eight-stranded C-terminal β -barrel. The two β -barrel structures are separated by a β -hairpin followed by two TM helices. A 22-residue loop links the TM helices to the C-terminal β -barrel. Residues from this loop participate in trimer interface interactions with the β -barrel structures from the adjacent protomer, whereas the β -hairpin is involved in intraprotomer stabilization. Notably, subunit II of cytochrome *c* oxidase, which contains the dinuclear Cu_A site, also comprises a soluble C-terminal β -barrel domain and two TM helices^{22,23} (Fig. 3). The pmoB subunit houses a dinuclear copper centre as well, in the N-terminal β -barrel (see below). The pmoB and subunit II β -barrels are not superimposable, however.

The pmoA and pmoC subunits reside primarily in the membrane. The pmoA subunit consists of seven TM helices and packs against the two TM helices from pmoB (Fig. 2a, c). These helices, which span the range of observed TM helix lengths²⁴, are inclined with respect to one another, and several are quite tilted with respect to the lipid bilayer normal. The two C-terminal helices face the opening at the trimer centre and interact with their counterparts from the other two protomers. A short helix and a β -hairpin structure protrude from the membrane, and interact with the soluble region of pmoB. pmoC comprises five TM helices that are oriented approximately parallel to the membrane normal and to one another (Fig. 2d). The four N-terminal TM helices average ~29 residues.

Metal centres

The crystal structure reveals three metal centres per protomer (Figs 2a and 4). The first site (Fig. 4a) is located in pmoB ~25 Å above the membrane and near the surface of the N-terminal β -barrel. The metal ion was assigned to be copper from the strong peaks in anomalous Fourier maps calculated using data collected near the copper ('CuANOM' in Supplementary Table S1) and zinc ('Highres' in Supplementary Table S1) absorption edges. Because the zinc absorption edge is higher in energy than the copper absorption edge, anomalous peaks attributable to copper appear in both maps (Fig. 4a). There is no evidence to suggest that this site contains more than one copper ion, and attempts to model additional copper ions were not consistent with anomalous Fourier maps. The copper ion is coordinated by the δ nitrogen atoms of His 48 and His 72 with a nearly linear geometry. Gln 404 is also within 3 Å of the copper ion. Whereas His 72 is highly conserved, His 48 is replaced with asparagine in *M. trichosporium* OB3b and *Methylocystis* sp. strain M pMMO. The assignment of this residue to be histidine is supported by the electron density and the presence of histidine in both the original pmoB gene sequence¹⁰ and the pmoB gene sequence from the *M. capsulatus* (Bath) genome²⁵. The codons for histidine and asparagine differ by a single nucleotide, so the difference may be due to a sequencing error. Alternatively, asparagine could coordinate the copper ion in the homologues.

This mononuclear copper centre resembles the type 2 site found in multicopper oxidases such as ascorbate oxidase and ceruloplasmin²⁶. In these enzymes, the copper ion is coordinated by the ϵ nitrogen atoms of two histidines and a water molecule, visible in all the structures except for the 3.1-Å resolution structure of ceruloplasmin. Solvent ligands may also be present in the pMMO site, but are not detected at 2.8-Å resolution. In accordance with these structural similarities, this copper centre probably gives rise to the type 2 Cu(II) EPR signal observed for purified pMMO^{13,14,16}. In the multicopper oxidases, the type 2 site is located proximal to a dinuclear type 3 site, forming a trinuclear cluster in which the copper ions are within 4–5 Å of one another²⁶. The type 3 site is also ligated by histidines. The surroundings of the pMMO mononuclear site indicate that this site is not a crystallographically depleted variant of the trinuclear multicopper oxidase site. There are no other histidine residues nearby, and the only potential metal binding residues, Gln 404 and Glu 75, are located near the protein surface ~2.7 Å and ~4 Å from the copper centre, respectively. These two residues, which are not conserved, are hydrogen-bonded to one another, and Glu 75 further interacts with pmoB in the neighbouring protomer.

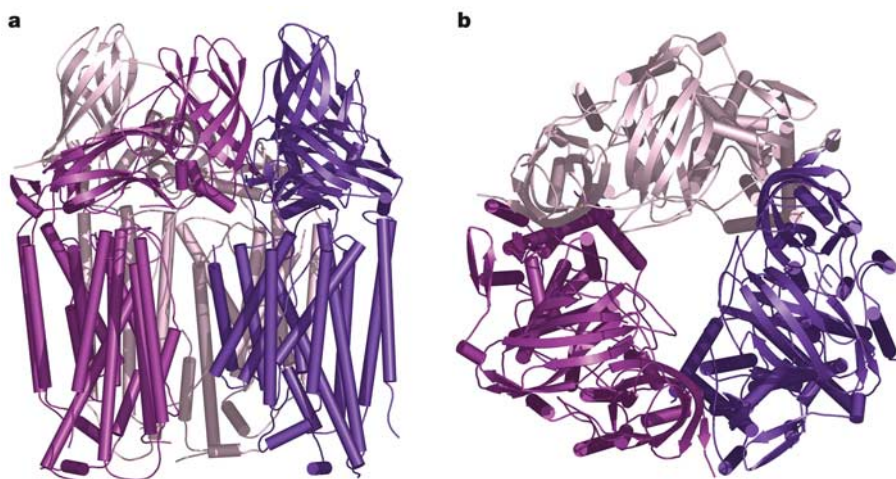


Figure 1 The pMMO trimer viewed parallel to the membrane normal (a) and perpendicular to the membrane normal (b). The three protomers are shown in dark purple, magenta, and light pink. Helices are represented as cylinders and β strands are represented as arrows.

The second copper site (Fig. 4b) is also contained within the N-terminal β -barrel of pmoB, ~ 21 Å from the mononuclear site (Figs 2a and 4). The location of this site, ~ 10 Å above the lipid bilayer interface, is similar to that of the cytochrome *c* oxidase Cu_A site^{22,23} (Fig. 3). We have modelled this site in pMMO as dinuclear on the basis of several observations. First, the electron density in the 3.0-Å resolution copper anomalous Fourier map has an oblong shape. Second and most important, two distinct peaks are observed at this site in a 2.8-Å resolution zinc anomalous Fourier map (Fig. 4b). The same map calculated to 3.0-Å resolution exhibits a single peak, suggesting that the resolution limits of the data are hindering detection of more than one copper ion.

Consistent with the 2.57-Å Cu–metal interaction determined by EXAFS¹³, the Cu–Cu distance in the dinuclear model refines to ~ 2.6 Å. If this site does indeed correspond to the site giving rise to the 2.57-Å Cu–metal interaction, the crystal structure confirms that the interacting metal ion is copper, not iron. No electron density was detected in iron anomalous Fourier maps generated with data sets collected at the iron absorption edge. Although we believe the dinuclear assignment is the best interpretation of the current data, it is also possible to refine the site with a single copper ion. By contrast, modelling three copper ions resulted in significant negative density in $F_o - F_c$ maps, indicating that this site does not

house the trinuclear cluster proposed by Chan and co-workers¹⁷. The oxidation state of the copper ions cannot be discerned from the structure, but a fluorescence scan of the crystal at the copper absorption edge exhibits a peak at $\sim 8,984$ eV. This characteristic Cu(I) feature was observed previously in our X-ray absorption near-edge structure (XANES) spectra¹³, and suggests that the crystals contain some Cu(I). If the mononuclear site generates the type 2 Cu(II) EPR signal, one or both of the copper ions in the dinuclear site is probably Cu(I).

In the dinuclear site, one copper ion is coordinated by the N-terminal residue of pmoB, His 33. Both the N-terminal amino nitrogen and the sidechain δ nitrogen are within coordinating distance. The second copper ion is ligated by the δ nitrogen of His 137 and the ϵ nitrogen of His 139 (Fig. 4b). These residues are highly conserved in pMMO and AMO from a number of organisms. Residues His 33 and His 139 are held in position by hydrogen bonds to the side chain of Glu 35 and the carbonyl oxygen of Gly 152, respectively. Both of these residues are also conserved. Additional terminal or bridging ligands may be present, but are not observed in the 2.8-Å-resolution electron density maps.

Coordination via the N-terminal amine is unusual but not unprecedented. In the bacterial nickel superoxide dismutase, bidentate chelation by the N-terminal amine and histidine side chain is

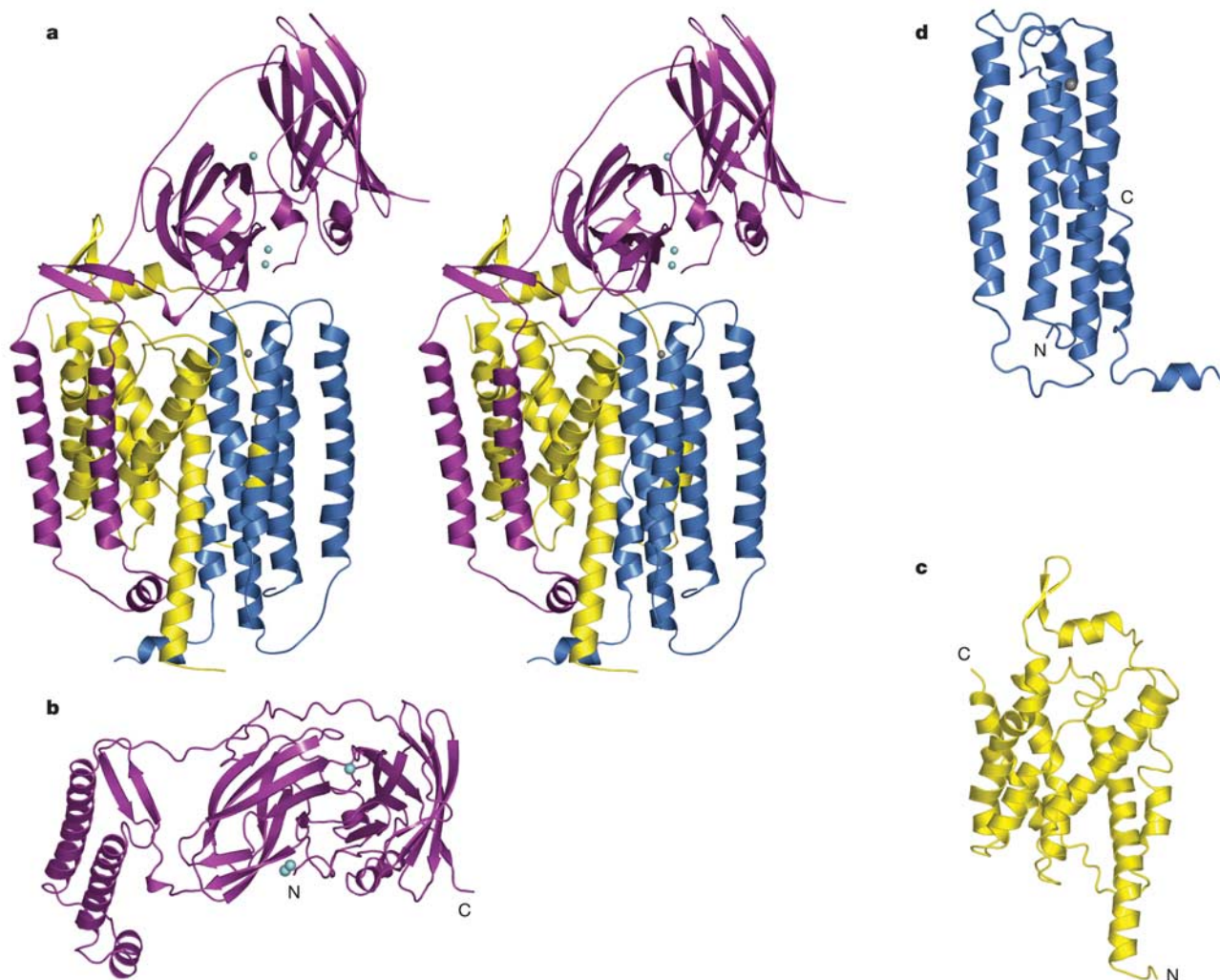


Figure 2 The pMMO subunits. **a**, Stereoview of a single protomer with pmoB shown in magenta, pmoA shown in yellow, and pmoC shown in blue. Copper ions are shown as cyan spheres, and a zinc ion is shown as a grey sphere. **b**, The pmoB subunit viewed

looking down the membrane normal. The N-terminal β -barrel is in the middle. **c**, The pmoA subunit. **d**, The pmoC subunit.

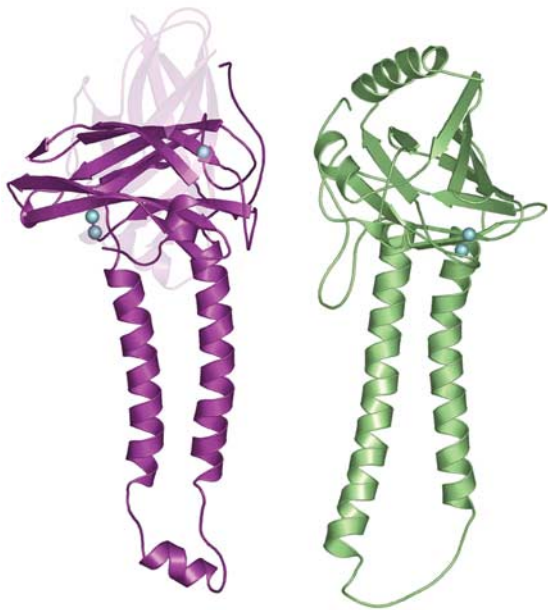


Figure 3 Comparison of pmoB (magenta) with *Paracoccus denitrificans* cytochrome *c* oxidase subunit II (green, PDB accession code 1AR1). The view was generated by superimposing the transmembrane helices and then translating the two proteins away from one another. The N-terminal pMMO β -barrel and the cytochrome *c* oxidase β -barrel are oriented differently. The C-terminal β -barrel of pmoB is transparent for clarity. Copper ions are shown as cyan spheres.

observed. In the proposed reaction mechanism, axial binding of the histidine δ nitrogen to Ni(III) tunes the reduction potential for superoxide dismutation²⁷. Activation of the enzyme requires proteolytic cleavage of a 14-residue leader sequence upstream of this histidine. Similarly, the N-terminal amino nitrogen of the photosynthetic cytochrome *f* subunit is axially bound to a haem iron²⁸. Analogous to cytochrome *f*, assembly of the pMMO dicopper site most probably occurs after the signal peptide is cleaved, when pmoB has already been translocated to the lipid bilayer. Finally, amino-terminal coordination of Cu(II) occurs in the amino-terminal Cu(II)- and Ni(II)-binding (ATCUN) motif, observed in albumin²⁹. We note, however, that the pmoB N terminus is not involved in copper binding if the site is modelled as mononuclear.

The third metal centre (Fig. 4c), modelled as a single zinc ion, is located within the lipid bilayer, ~ 19 Å from the dinuclear copper centre (Figs 2a and 4). The three related sites in the pMMO trimer represent the highest peaks in a zinc anomalous Fourier map, and are not present in anomalous maps calculated using data collected at the lower-energy copper edge. Several additional zinc ions mediate crystal lattice contacts. The zinc ion is coordinated in a distorted tetrahedral geometry by conserved residues Asp 156, His 160 and His 173 from pmoC, and Glu 195 from pmoA (Fig. 4c). This glutamic acid residue can only be tentatively assigned owing to a disordered loop and poor side-chain electron density for residues 193–244. Alternate ligands include Glu 199 and Met 201 from pmoA. Metal analysis by inductively coupled plasma atomic emission spectroscopy (ICP-AES) indicates that pMMO samples contain less than 0.2 moles of zinc per 100 kDa before crystallization. The zinc in this site is therefore derived from zinc acetate in the crystallization buffer. Although this site could be adventitious, it is probably occupied by another metal ion *in vivo* such as copper or iron.

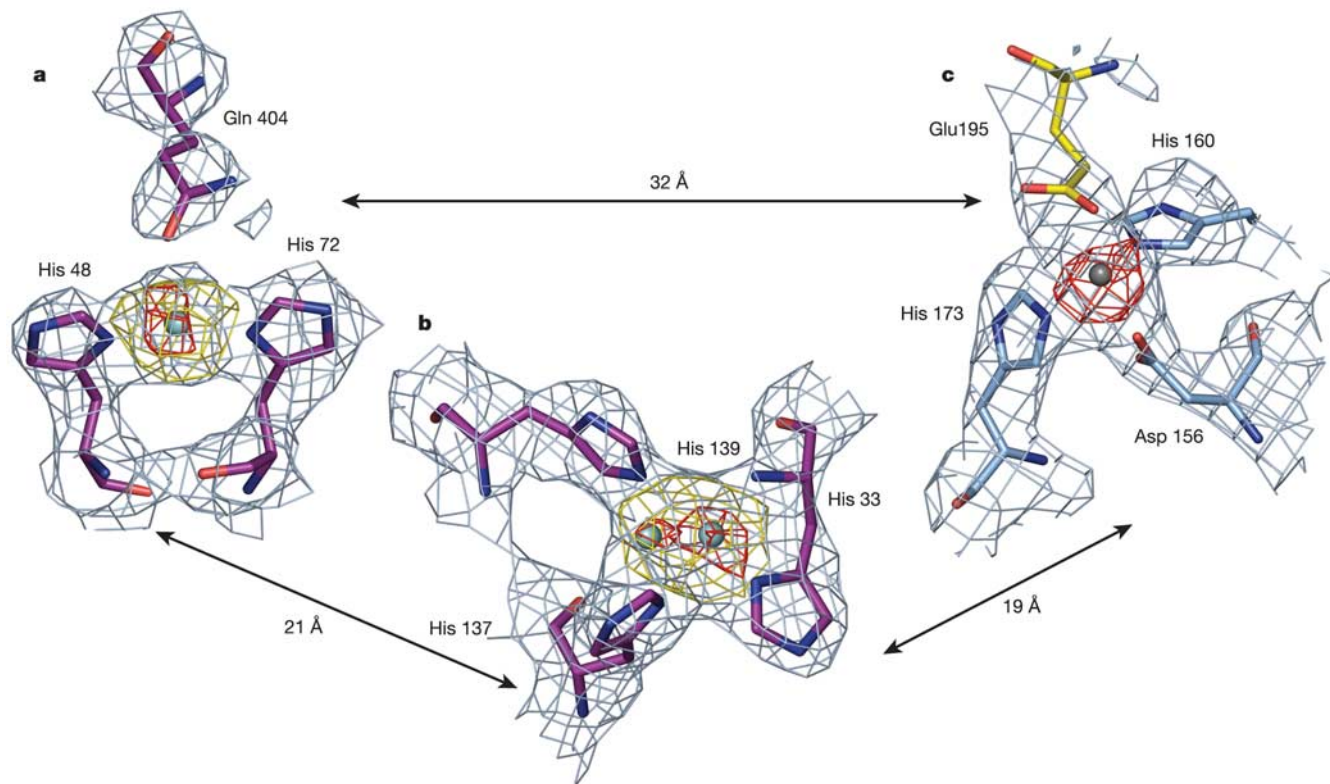


Figure 4 The pMMO metal centres viewed approximately 90° from the orientation shown in Fig. 2a. The distances are measured between metal ions. Anomalous difference Fourier maps calculated using data collected near the copper absorption edge (yellow,

'CuANOM', contoured at 4σ) and near the zinc absorption edge (red, 'Highres', contoured at 4σ) are superimposed on the final $2F_o - F_c$ electron density map (light blue, contoured at 1σ). **a**, The mononuclear copper site. **b**, The dinuclear copper site. **c**, The zinc site.

Taken together, the three metal centres give a stoichiometry of three copper ions and a fourth yet-to-be-identified metal ion per 100 kDa $\alpha\beta\gamma$ protomer, consistent with values measured previously for *M. capsulatus* (Bath) pMMO by us¹³ and Dalton and co-workers¹⁶, but significantly different from the 12–15 copper ions reported by Chan and co-workers¹⁷. One potential explanation is that additional copper binding sites, not occupied in the crystal, are present. Histidine ligation of the trinuclear C-clusters was predicted based on electron spin echo modulation spectroscopic (ESEEM) data for *M. capsulatus* (Bath) membrane samples³⁰. An inspection of all the histidine residues, both conserved and nonconserved, in the pMMO protomer does not reveal any obvious metal binding sites. There is one cluster of primarily hydrophilic residues ~ 13 Å from the zinc site. This region includes conserved residues His 38, Met 42, Asp 47, Asp 49 and Glu 100 from pmoA and Glu 154 from pmoC. These residues may be involved in protomer stabilization, but it is conceivable that they could form a quinone or metal binding site. It is most likely, however, that the observed metal centres represent the only metal binding sites in pMMO.

Functional implications

Oxygen binding, activation and subsequent substrate oxidation have been studied extensively for copper proteins and synthetic model complexes³¹. The nuclearity of biological copper centres is not correlated with reactivity, leaving open the possibility that any one of the pMMO sites could be catalytic. The dinuclear centre (Fig. 4b) is an attractive candidate for the active site because it is unusual. Other dicopper centres, including those in haemocyanin, tyrosinase, and catechol oxidase, can bind and/or activate dioxygen. Whereas haemocyanin only binds dioxygen reversibly, the latter two enzymes hydroxylate tyrosine and convert catechol to quinone, respectively. The Cu–Cu separation in these enzymes is significantly greater than that in pMMO, and each copper ion in haemocyanin and catechol oxidase is coordinated by three histidines³¹ rather than one or two in pMMO. In support of methane binding at the dinuclear site, there is an adjacent cavity lined by several conserved hydrophobic residues including Pro 94 from pmoB and Leu 78, Ile 163, and Val 164 from pmoC. A second cavity involving some of the same residues extends almost to the zinc site.

Alternatively, structural similarities between pmoB and cytochrome *c* oxidase subunit II could indicate that the dinuclear site functions in electron transfer. The copper ions in this site are ~ 20 Å from the other metal ions in the same protomer and >40 Å from the metal sites in the other protomers. Within one protomer, the minimum distance between atoms directly coordinated to these two copper ions and atoms directly coordinated to the mononuclear copper and zinc ions is ~ 14 Å, which is reasonable for electron transfer³². Notably, the side chain of conserved residue pmoB Trp 156 shields the dinuclear copper centre from the solvent. An analogous surface tryptophan in cytochrome *c* oxidase²² has been implicated in electron transfer from cytochrome *c* to the Cu_A site³³. The coordination environment of the pmoB dinuclear site differs from that of Cu_A, however. In Cu_A, the two copper ions are bridged by two cysteine sulphur atoms and terminally coordinated by two histidines, a methionine and a carbonyl oxygen. Key features of Cu_A that contribute to the electron transfer function and are not observed in pMMO include complete delocalization of electrons and the high covalency of the Cu–S(Cys) bonds³⁴.

If the dinuclear site is involved in electron transfer, the mononuclear site (Fig. 4a) might be catalytic. The mononuclear copper centres in peptidylglycine α -hydroxylating monooxygenase (PHM) and dopamine β -monooxygenase (D β M) catalyse hydroxylation of a glycine C α –H bond and a dopamine benzylic C–H bond, respectively³⁵. In these enzymes, a Cu(II)-superoxo complex is proposed to abstract a hydrogen atom from the substrate³⁶. The copper ion is ligated by two histidines and a methionine, which is essential for reactivity³⁵. The pMMO site could exhibit similar

reactivity, although a methionine ligand is not present. In PHM, an additional electron is provided by a second mononuclear copper site located ~ 11 Å away.

In addition, we cannot exclude the possibility that the zinc site (Fig. 4c) is the active site. In cytochrome *c* oxidase, the catalytic centre is located ~ 13 Å within the membrane ~ 20 Å from the electron transfer Cu_A site²³. Multiple combinations of the zinc ligands and proximal residues could provide ligands to either a third copper centre or an iron centre. If Met 201 from pmoA is involved, a copper site similar to that in PHM could assemble. There are only two nearby histidines, so a multinuclear copper site seems unlikely at this position. Finally, it has not escaped our attention that a carboxylate-bridged di-iron centre, similar to that in MMOH⁸, could be accommodated at this position. Two additional nearby carboxylate residues, Asp 168 and Glu 176 from pmoC, could complete the coordination sphere. These two residues are conserved among pMMO homologues, but not in the related AMO. Canonical iron binding motifs³⁷ are not present in the pMMO sequence, however, and no spectroscopic data suggestive of a di-iron centre have been obtained.

The physiological source of electrons for any of the pMMO metal sites is unknown. Exogenous quinones have been shown to stimulate NADH-dependent pMMO activity in solubilized membranes. Shiemke and co-workers have proposed that a type 2-NADH:quinone oxidoreductase (NDH-2) uses NADH generated by oxidation of formate and formaldehyde to reduce endogenous quinones. These resultant quinols could then reduce pMMO either directly or through an additional yet-to-be-identified reductase³⁸. There is a nonprotein patch of strong electron density near the interface between the two pmoB β -barrels and ~ 13 Å from both the copper centres that could accommodate a quinol (Supplementary Fig. S1). The structure also reveals a possible docking site for NDH-2 or other reductases, a negatively charged patch on the outer surface of the soluble domains of pmoB close to the dinuclear copper site (Supplementary Fig. S2). This region includes conserved residues pmoB Glu 35, pmoB Asp 368, and pmoC Asp 45. A cluster of acidic residues also forms the proposed docking site for cytochrome *c* on cytochrome *c* oxidase³⁹.

In conclusion, the pMMO structure reveals an unexpected trimeric arrangement and the overall folds of the three subunits. Two of the three metal centres, modelled as mononuclear and dinuclear copper, are located within the soluble regions of the pmoB subunit. The third metal centre, occupied by zinc in the crystal, lies within the membrane with ligands derived from both pmoC and pmoA. Direct electron transfer between metal centres may be possible. Neither the site of methane oxidation nor the pathway(s) of substrate entry and product egress have yet been identified. Studies to address these issues are underway, and will provide a foundation for future studies of the pMMO methane oxidation mechanism. □

Methods

Protein purification and crystallization

Methylococcus capsulatus (Bath) cultures were fermented and the membranes isolated as described previously¹³. pMMO was purified in the presence of the detergent undecyl- β -D-maltoside (Anatrace) by ammonium sulphate precipitation followed by anion exchange chromatography on a Source 30Q (Amersham Biosciences) column. Purified pMMO was exchanged into 50 mM HEPES pH 7.5 containing 0.12% Cymal-5 (Anatrace) by fourfold dilution and concentration using a microcon YM-100 (Millipore). As described previously, most samples were not active¹³. Crystals were grown at room temperature in clover-leaf sitting drop trays (DeCode Biostructures) by mixing 1 μ l of ~ 20 mg ml⁻¹ pMMO with 1 μ l precipitant solution containing 200 mM zinc acetate and 8–12% PEG 8000. Colourless rod-shaped crystals with final dimensions of $\sim 100 \times 100 \times 400$ μ m appeared after 1–2 weeks. Activity assays were not attempted on the crystals owing to insufficient quantities. Crystals were flash-frozen using 15% ethylene glycol as a cryoprotectant.

Structure determination and refinement

The structure was solved by copper SAD (Supplementary Table S1). All data sets were collected at the DND-CAT beamline at the Advanced Photon Source using a 3K \times 3K Mar

charge-coupled device (CCD) detector and processed with XDS⁴⁰ and SCALA⁴¹. Six copper sites were located using SOLVE⁴². A figure of merit of 0.24 was obtained for data in the 30–4.0-Å resolution range. High redundancy was critical to locating the copper sites, and was achieved by merging three complete data sets collected at the same energy on the same crystal ('CuSAD' in Supplementary Table S1). An interpretable electron density map was obtained from RESOLVE⁴³ following threefold noncrystallographic symmetry averaging, density modification using a solvent content of 70%, and phase extension to 2.8 Å resolution ('Highres' in Supplementary Table S1). Model building and adjustment was performed with XtalView⁴⁴. Approximately 85 iterative refinement cycles with CNS⁴⁵ followed by model rebuilding were performed. Translation liberation screw-rotation (TLS) parameters and restrained refinement options in REFMAC5⁴⁶ were used for the final refinement cycles. Noncrystallographic symmetry restraints were imposed throughout the refinement. The asymmetric unit contains one pMMO trimer.

The model includes all three pMMO subunits, pmoA, pmoB and pmoC, numbered according to the translated protein sequences for the genes *pmoA2*, *pmoB2* and *pmoC2*¹. Few sequence differences exist between the two pMMO gene copies in *M. capsulatus* (Bath). We chose the second gene copy based on the electron density for residue 173 in a well-defined region of pmoA. The density at this position is more consistent with tyrosine (*pmoA2*) than asparagine (*pmoA*). Several regions of pmoA and pmoC proved difficult to model, including the six N-terminal residues of pmoA and the 44 N-terminal residues of pmoC, which may be a leader sequence. Owing to a disordered loop comprising residues 193–195 and poor side chain density, residues 193–244 of pmoA are tentatively assigned, and the final 3 C-terminal residues are not modelled. In pmoC, residues 204–230 and 260–289 are not visible, and residues 231–259 are tentatively assigned. The final model consists of 2,424 amino acid residues, nine copper ions, and eight zinc ions. A Ramachandran plot calculated with PROCHECK⁴¹ indicates that 95.6%, 97.2% and 97.1% of the residues in pmoA, pmoB and pmoC, respectively, are in the most favoured and additional allowed regions. Figures were generated with PyMOL⁴⁷ and GRASP⁴⁸.

Received 9 November 2004; accepted 5 January 2005; doi:10.1038/nature03311.

Published online 26 January 2005.

1. Periana, R. A. *et al.* Perspectives on some challenges and approaches for developing the next generation of selective, low temperature, oxidation catalysts for alkane hydroxylation based on the CH activation reaction. *J. Mol. Catal. A* **220**, 7–25 (2004).
2. Periana, R. A. *et al.* A mercury-catalyzed, high-yield system for the oxidation of methane to methanol. *Science* **259**, 340–343 (1993).
3. Hanson, R. S. & Hanson, T. E. Methanotrophic bacteria. *Microbiol. Rev.* **60**, 439–471 (1996).
4. Park, S., Brown, K. W. & Thomas, J. C. The effect of various environmental and design parameters on methane oxidation in a model biofilter. *Waste Manag. Res.* **20**, 434–444 (2002).
5. Sullivan, J. P., Dickinson, D. & Chase, C. A. Methanotrophs, *Methylosinus trichosporium* OBBb, sMMO, and their application to bioremediation. *Crit. Rev. Microbiol.* **24**, 335–373 (1998).
6. Merckx, M. *et al.* Dioxygen activation and methane hydroxylation by soluble methane monooxygenase: a tale of two irons and three proteins. *Angew. Chem. Int. Edn Engl.* **40**, 2782–2807 (2001).
7. Arp, D. J., Sayavedra-Soto, L. A. & Hommes, N. G. Molecular biology and biochemistry of ammonia oxidation by *Nitrosomonas europaea*. *Arch. Microbiol.* **178**, 250–255 (2002).
8. Rosenzweig, A. C., Frederick, C. A., Lippard, S. J. & Nordlund, P. Crystal structure of a bacterial non-haem iron hydroxylase that catalyses the biological oxidation of methane. *Nature* **366**, 537–543 (1993).
9. Lieberman, R. L. & Rosenzweig, A. C. Biological methane oxidation: regulation, biochemistry, and active site structure of particulate methane monooxygenase. *Crit. Rev. Biochem. Mol. Biol.* **39**, 147–164 (2004).
10. Semrau, J. D. *et al.* Particulate methane monooxygenase genes in methanotrophs. *J. Bacteriol.* **177**, 3071–3079 (1995).
11. Stolyar, S., Costello, A. M., Peeples, T. L. & Lidstrom, M. E. Role of multiple gene copies in particulate methane monooxygenase activity in the methane-oxidizing bacterium *Methylococcus capsulatus* Bath. *Microbiology* **145**, 1235–1244 (1999).
12. Yu, S. S.-F. *et al.* Production of high-quality particulate methane monooxygenase in high yields from *Methylococcus capsulatus* (Bath) with a hollow-fiber membrane bioreactor. *J. Bacteriol.* **185**, 5915–5924 (2003).
13. Lieberman, R. L. *et al.* Purified particulate methane monooxygenase from *Methylococcus capsulatus* (Bath) is a dimer with both mononuclear copper and a copper-containing cluster. *Proc. Natl Acad. Sci. USA* **100**, 3820–3825 (2003).
14. Choi, D. W. *et al.* The membrane-associated methane monooxygenase pMMO and pMMO-NADH:quinone oxidoreductase complex from *Methylococcus capsulatus* Bath. *J. Bacteriol.* **185**, 5755–5764 (2003).
15. Nguyen, H. H., Elliott, S. J., Yip, J. H. & Chan, S. I. The particulate methane monooxygenase from *Methylococcus capsulatus* (Bath) is a novel copper-containing three-subunit enzyme. Isolation and characterization. *J. Biol. Chem.* **273**, 7957–7966 (1998).
16. Basu, P., Katterle, B., Andersson, K. K. & Dalton, H. The membrane-associated form of methane monooxygenase from *Methylococcus capsulatus* (Bath) is a copper/iron protein. *Biochem. J.* **369**, 417–427 (2003).
17. Chan, S. I., Chen, K. H.-C., Yu, S. S.-F., Chen, C.-L. & Kuo, S. S.-J. Toward delineating the structure and function of the particulate methane monooxygenase from methanotrophic bacteria. *Biochemistry* **43**, 4421–4430 (2004).
18. Lemos, S. S., Yuan, H. & Perille-Collins, M. L. Review of multifrequency EPR of copper in particulate methane monooxygenase. *Curr. Top. Biophys.* **26**, 43–48 (2002).
19. Kim, H. J. *et al.* Methanobactin, a copper-acquisition compound from methane oxidizing bacteria. *Science* **305**, 1612–1615 (2004).

20. le Maire, M., Champeil, P. & Møller, J. V. Interaction of membrane proteins and lipids with solubilizing detergents. *Biochim. Biophys. Acta* **1508**, 86–111 (2000).
21. Tsuprun, V. L. *et al.* Electron microscopy of methane monooxygenase of the methane-oxidizing bacterium *Methylococcus capsulatus*. *Dokl. Akad. Nauk SSSR* **292**, 490–493 (1987).
22. Iwata, S., Ostermeier, C., Ludwig, B. & Michel, H. Structure at 2.8 Å resolution of cytochrome c oxidase from *Paracoccus denitrificans*. *Nature* **376**, 660–669 (1995).
23. Tsukihara, T. *et al.* Structures of the metal sites of oxidized bovine heart cytochrome c oxidase at 2.8 Å. *Science* **269**, 1069–1074 (1995).
24. Bowie, J. U. Helix packing in membrane proteins. *J. Mol. Biol.* **272**, 780–789 (1997).
25. Ward, N. *et al.* Genomic insights into methanotrophy: the complete genome sequence of *Methylococcus capsulatus* (Bath). *PLoS Biol.* **2**, e303 (2004).
26. Solomon, E. I., Sundaram, U. M. & Machonkin, T. E. Multicopper oxidases and oxygenases. *Chem. Rev.* **96**, 2563–2605 (1996).
27. Barondeau, D. P., Kassmann, C. J., Bruns, C. K., Tainer, J. A. & Getzoff, E. D. Nickel superoxide dismutase structure and mechanism. *Biochemistry* **43**, 8038–8047 (2004).
28. Martinez, S. E., Huang, D. S., Szczepaniak, A., Cramer, W. A. & Smith, J. L. Crystal structure of chloroplast cytochrome *f* reveals novel cytochrome fold and unexpected heme ligation. *Structure* **2**, 95–105 (1994).
29. Harford, C. & Sarkar, B. Amino terminal Cu(II)- and Ni(II)-binding (ATCUN) motif of proteins and peptides: metal binding, DNA cleavage, and other properties. *Acc. Chem. Res.* **30**, 123–130 (1997).
30. Elliott, S. J., Randall, D. W., Britt, R. D. & Chan, S. I. Pulsed EPR studies of particulate methane monooxygenase from *Methylococcus capsulatus* (Bath): evidence for histidine ligation. *J. Am. Chem. Soc.* **120**, 3247–3248 (1998).
31. Mirica, L. M., Ottenwaelder, X. & Stack, T. D. P. Structure and spectroscopy of copper-dioxygen complexes. *Chem. Rev.* **104**, 1013–1045 (2004).
32. Gray, H. B. & Winkler, J. R. Electron tunneling through proteins. *Q. Rev. Biophys.* **36**, 341–372 (2003).
33. Witt, H., Malatesta, F., Nicoletti, F., Brunori, M. & Ludwig, B. Tryptophan 121 of subunit II is the electron entry site to cytochrome-c oxidase in *Paracoccus denitrificans*. *J. Biol. Chem.* **273**, 5132–5136 (1998).
34. George, S. D. *et al.* A quantitative description of the ground-state wave function of Cu_A by X-ray absorption spectroscopy: comparison to plastocyanin and relevance to electron transfer. *J. Am. Chem. Soc.* **123**, 5757–5767 (2001).
35. Prigge, S. T., Mains, R. E., Eipper, B. A. & Amzel, L. M. New insights into copper monooxygenases and peptide amidation: structure, mechanism and function. *Cell. Mol. Life Sci.* **57**, 1236–1259 (2000).
36. Chen, P. & Solomon, E. I. O₂ activation by binuclear Cu sites: noncoupled versus exchange coupled reaction mechanisms. *Proc. Natl Acad. Sci. USA* **101**, 13105–13110 (2004).
37. Nordlund, P. & Eklund, H. Di-iron-carboxylate proteins. *Curr. Opin. Struct. Biol.* **5**, 758–766 (1995).
38. Cook, S. A. & Shiemke, A. K. Evidence that a type-2 NADH:quinone oxidoreductase mediates electron transfer to particulate methane monooxygenase in *Methylococcus capsulatus*. *Arch. Biochem. Biophys.* **398**, 32–40 (2002).
39. Maneg, O., Malatesta, F., Ludwig, B. & Drosou, V. Interaction of cytochrome c with cytochrome oxidase: two different docking scenarios. *Biochim. Biophys. Acta* **1655**, 274–281 (2004).
40. Kabsch, W. Automatic processing of rotation diffraction data from crystals of initially unknown symmetry and cell constants. *J. Appl. Crystallogr.* **26**, 795–800 (1993).
41. Collaborative Computational Project Number 4. The CCP4 suite programs for protein crystallography. *Acta Crystallogr. D* **50**, 760–763 (1994).
42. Terwilliger, T. C. & Berendzen, J. Automated MAD and MIR structure solution. *Acta Crystallogr. D* **55**, 849–861 (1999).
43. Terwilliger, T. C. Automated main-chain model building by template matching and iterative fragment extension. *Acta Crystallogr. D* **59**, 34–44 (2002).
44. McRee, D. E. XtalView Xfit—a versatile program for manipulating atomic coordinates and electron density. *J. Struct. Biol.* **125**, 156–165 (1999).
45. Brünger, A. T. *et al.* Crystallography & NMR system: a new software suite for macromolecular crystallography. *Acta Crystallogr. D* **54**, 905–921 (1998).
46. Winn, M. D., Isupov, M. N. & Murshudov, G. N. Use of TLS parameters to model anisotropic displacements in macromolecular refinement. *Acta Crystallogr. D* **57**, 122–133 (2001).
47. Delano, W. L. *The PyMOL Molecular Graphics System* (DeLano Scientific, San Carlos, California, 2002).
48. Nicholls, A., Sharp, K. A. & Honig, B. Protein folding and association: insights from the interfacial and thermodynamic properties of hydrocarbons. *Proteins* **11**, 281–296 (1991).

Supplementary Information accompanies the paper on www.nature.com/nature.

Acknowledgements This work was supported by a grant from the American Chemical Society Petroleum Research Fund (A.C.R.), funds from the David and Lucile Packard Foundation (A.C.R.), and the NIH (A.C.R.). R.L.L. was supported in part by a NIH training grant. We thank D. Shrestha for assistance cultivating *M. capsulatus* (Bath), M. Sommerhalter for assistance with data collection, J. Brunzelle for suggestions, Z. Wawrzak for assistance with data collection, and B. Hoffman, T. Stemmler, and K. Karlin for discussions.

Competing interests statement The authors declare that they have no competing financial interests.

Correspondence and requests for materials should be addressed to A.C.R. (amy@northwestern.edu). Coordinates have been deposited in the Protein Data Bank (accession code 1YEW).